Physics of Fluids

Alcove formation in dissolving cliffs driven by density inversion instability

Cite as: Phys. Fluids **34**, 054118 (2022); https://doi.org/10.1063/5.0092331
Submitted: 22 March 2022 • Accepted: 05 May 2022 • Accepted Manuscript Online: 06 May 2022 • Published Online: 25 May 2022

Ram Sudhir Sharma, Michael Berhanu and Arshad Kudrolli

Physics of Fluids ARTICLE scitation.org/journal/phf

Alcove formation in dissolving cliffs driven by density inversion instability

Cite as: Phys. Fluids **34**, 054118 (2022); doi: 10.1063/5.0092331
Submitted: 22 March 2022 · Accepted: 5 May 2022 ·
Published Online: 25 May 2022

Ram Sudhir Sharma,[1] Michael Berhanu,[2] and Arshad Kudrolli[1,a)]

AFFILIATIONS

[1]Department of Physics, Clark University, Worcester, Massachusetts 01610, USA
[2]MSC, Université Paris Cité (UMR 7057), F-75013 Paris, France

[a)]Author to whom correspondence should be addressed: akudrolli@clarku.edu

ABSTRACT

We demonstrate conditions that give rise to cave-like features commonly found in dissolving cliffsides with a minimal two-phase physical model. Alcoves that are wider at the top and tapered at the bottom, with sharp-edged ceilings and sloping floors, are shown to develop on vertical solid surfaces dissolving in aqueous solvents. As evident from descending plumes, sufficiently large indentations evolve into alcoves as a result of the faster dissolution of the ceiling due to a solutal Rayleigh–Bénard density inversion instability. In contrast, defects of size below the boundary layer thickness set by the critical Rayleigh number smooth out, leading to stable planar interfaces. The ceiling recession rate and the alcove opening area evolution are shown to be given to first-order by the critical Rayleigh number. By tracking passive tracers in the fluid phase, we show that the alcoves are shaped by the detachment of the boundary layer flow and the appearance of a pinned vortex at the leading edge of the indentations. The attached boundary layer past the developing alcove is then found to lead to rounding of the other sides and the gradual sloping of the floor.

I. INTRODUCTION

The coupled evolution of solid–fluid interfaces due to dissolution, melting, and erosion is important in shaping geophysical features including mountains, icebergs, caverns, aquifers, and petroleum reservoirs.[1–4] While typically slow, such evolution can lead to dramatic appearance of sinkholes, avalanches, and other modes of rapid failure. There is considerable need to understand the evolution of such features from a mechanistic perspective to complement field observations toward developing quantitative models because of their complexity and ubiquity both on Earth and other celestial bodies.[3,5,6]

Irregular surface patterns in salt crystals dissolving from below in aqueous solutions have been observed and analyzed with turbulent boundary layer models.[7,8] Differential growth resulting in up-facing conical cavities created within salt deposits shaped by dissolution driven internal flows has been investigated in the context of land subsidence and structure collapse.[9] Opacity of the medium only allowed intermittent and indirect inferences to be drawn in these studies. Recent studies of two-phase model systems with rapidly dissolving non-crystalline hard candy have illuminated the formation of pinnacles in karsts, furrows in sandstone, and ice scallops.[10–17] Significant progress has been made in describing the observed outer envelops of the structures with counter-intuitive growth of singularities vs blunting of sharp tips depending on the shapes of the initial surfaces and flow conditions.[15,18,19] While occurrence of surface cavities was noted as an undesirable outcome in their studies, they were not explored. Moreover, cavity growth is of interest in an even broader class of systems, as in fluid-mediated pitting corrosion that leads to deep isolated holes and failure in metal structures.[20]

Here, we focus on the evolution of vertical solid–liquid interfaces as a result of coupled fluid flow and dissolution of a solid. Figure 1 shows motivational examples of alcoves—cave-like features that occur above ground on cliffs—found in the American Southwest and thought to result from fluid flow and weathering. Dissolution of calcium carbonate and the repeated freezing and expansion cycles that weaken and loosen pieces are known to lead to alcoves within the cliffs as they erode. However, the minimal conditions under which they can occur and the detailed mechanism by which they evolve beyond these general descriptions remain unclear.

Therefore, we investigate if alcoves can be produced by using a highly simplified two-phase model composed of a homogeneous non-crystalline solid and a dissolving fluid phase in a gravitational field. The relatively high transparency and dissolution speed of the medium

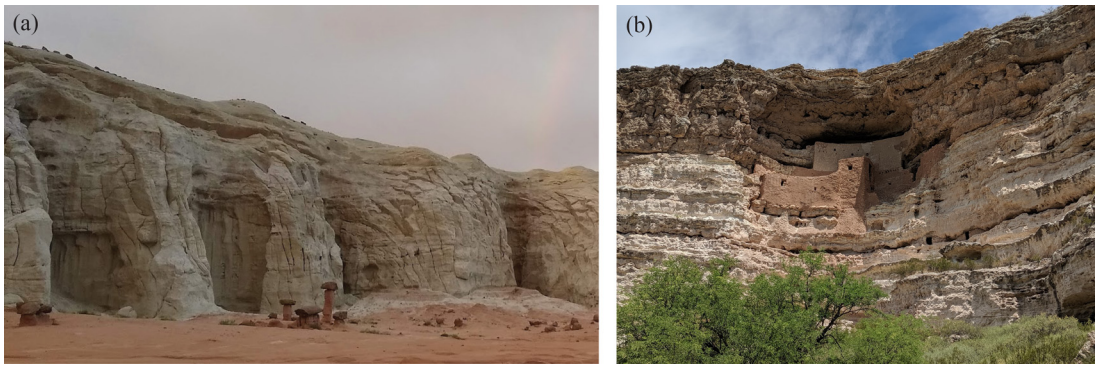

FIG. 1. Examples of alcoves observed in (a) Grand Staircase-Escalante National Monument, Utah, and (b) Montezuma Castle National Monument, Arizona, which has pre-Columbian dwellings built within. The cliffs are approximately 20 and 30 m high for scale, respectively. Photos taken on June 21, 2019 and June 24, 2019, respectively.

enable us to obtain detailed evolution information on the shapes with complementary optical and x-ray measurements and the flow fields in a matter of hours if not a day. Specifically, we show perturbations in a vertical dissolving interface develop into alcoves shaped by the interactions with the surrounding fluid as a result of a density inversion instability at the underside of surface perturbations. In contrast, up-facing horizontal surfaces are observed to dissolve more uniformly and much more slowly, even when surface indentations and material defects are present, under otherwise similar conditions.

II. MATERIALS AND METHODS

The solids used in our study are prepared with five part sucrose, three part light corn syrup, and two part distilled water by volume, similar to recipes in other studies.[10,13] These ingredients are stirred and heated together, while keeping the temperature at approximately 160 °C, until 7/8th of the original volume remains after evaporation corresponding to a density of $1.3 \pm 0.1\,\mathrm{g/cm^3}$. The hot liquid is poured into a 3D printed rectangular transparent mold with internal width W, length L, and height H. Typically, we use $W = 4\,\mathrm{cm}$, length $L = 6\,\mathrm{cm}$, and height $H = 0.3\,\mathrm{cm}$ to standardize our measurements and larger molds to check any mold dimension dependence. The hot liquid solidifies with a flat surface in gravity with prescribed surface indentations imposed as needed during the final stages of cooling as the glass transition is approached. Air bubbles from sub micrometer to a few millimeters in size generated during the mixing and heating process can be trapped in, and on, the surface of the hot liquid at it cools. The larger visible bubbles were eliminated by trial and error and degassing as needed. Surface indentations are also added if desired as the liquid hardens using solid impalers with prescribed shapes. Using this preparation method, we obtain a homogeneous noncrystalline solid with a uniform shade of color and density $\rho_s = 1.41 \pm 0.06\,\mathrm{g/cm^3}$.

The mold with solid within is then placed in a transparent acrylic rectangular container filled with distilled water and oriented as desired with one surface exposed. A surfactant is added to reduce air bubbles in the fluid. A sufficiently large bath is used so that density of the bath solution even after all the solid dissolves varied by less than 0.5%. The experiments were performed in a laboratory with temperature T in the range 21–25.1 °C as noted. The solid is imaged with a megapixel Pixelink color camera through the sidewalls of the container by backlighting with a uniform LED panel. The image intensity is mapped to the thickness of the solid enabling us to obtain a map of the surface dynamically (see Appendix A). The optical measurements are also complemented with snapshots of the solid with a Varian Medical Systems micro x-ray CT instrument. This requires us to pull the solid and the mold out of the bath and was mostly conducted to illustrate and check the overall shape of partially dissolved solids.

III. OBSERVATION OF ALCOVE GROWTH

Figure 2(a) shows an example of a surface prepared with two large circular indentations besides a number of smaller surface imperfections formed during the molding process. The solid and the mold are immersed while oriented vertically in the center of a bath container for 60 minutes as shown schematically in Fig. 2(b). An image of the partially dissolved solid, where a number of pits or alcove-like features have appeared, is shown in Fig. 2(c). Comparing Fig. 2(a) and Fig. 2(c), the largest alcoves correspond to the two initial circular indentations, but many other smaller ones are also observed. A surface rendering of a typical alcove obtained with x-ray scanning—corresponding to the region indicated by Fig. 2(c)—is shown in Figs. 2(d) and 2(e) as viewed at a 60° angle and from the side, respectively. A sharp transition from the vertical interface to the ceiling can be observed, whereas the floor is very sloped and meets the vertical interface with a further gradual change of slope. The alcoves are wider near the top and appear conical below, giving rise to an overall inverted triangle appearance with flat ceilings, reminiscent of the alcoves seen in Fig. 1.

From a snapshot alone, it is difficult to match each of the alcoves with a defect, but it is evident that defects play an important part in their formation. Therefore, we performed complementary experiments with a $6 \times 4 \times 0.3\,\mathrm{cm^3}$ solid with an initial 0.1 cm fluid filled gap between the dissolving interface and container boundary to enable clear visualization. Figure 3(a) shows the evolution of the outline and vertical transect of an alcove observed using optical imaging at various stages of development. The calibration used to map the image intensity to the local surface height can be found in Appendix A. The corresponding movie can be found in the supplementary material. Here, an essentially flat surface is observed to develop an alcove which grows longer, wider, and deeper until it encounters the back wall of the mold. Even beyond that point, the alcove is observed to continue to grow longer and wider. Thus, the alcove is observed to evolve to have an inverted triangle appearance with a sharp transition to the horizontal

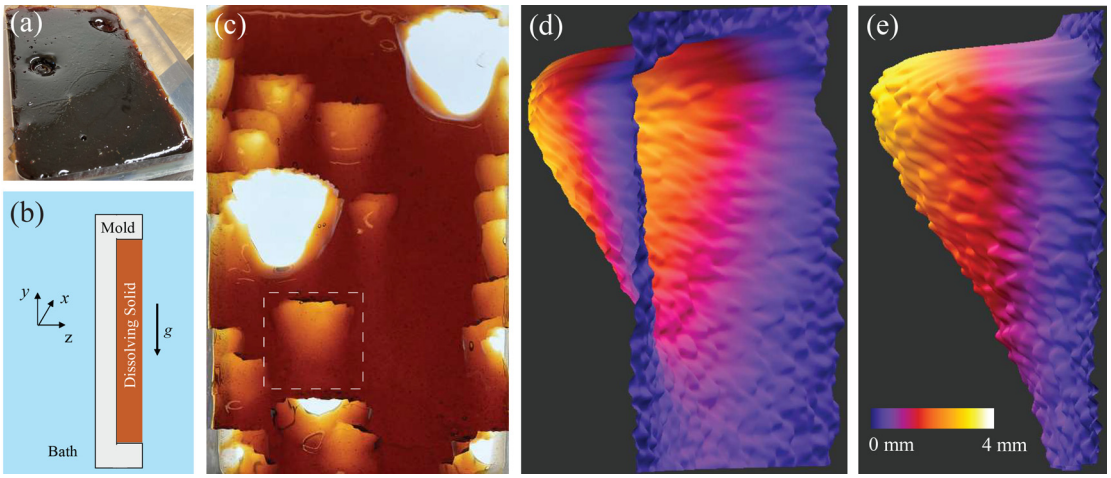

FIG. 2. (a) Image of solid sugar block with two circular indentations contained within a transparent mold. ($L = 14$; $W = 9$; and $H = 1$ cm). Several other small and large defects are also made visible by reflected light. (b) Schematic cross section of the sugar block contained within the mold placed vertically in an aqueous bath and the Cartesian coordinate system. (c) The surface shows development of a number of alcoves after being immersed for an hour. (d) A surface rendering obtained with x-ray scanning displayed at a 60°. The alcove shown corresponds to the one marked with the dashed box corresponding to a 3×3 cm^2 area in (c). (e) Same surface plot shown from side.

roof from the vertical face and a smooth sloping floor, which gradually transitions to the vertical surface similar to that shown in Figs. 2(d) and 2(e).

This evolution indicates that all the alcove-like features observed in Fig. 2(c) are similar in nature, and the smaller ones start to form later as the dissolving interface reaches small air bubbles trapped inside the dissolving solid. While some surface indentations develop into alcoves, adjacent vertical regions become optically smooth compared to even the initial surface, which may have small pits and grooves on the solid surface formed during the cooling process. Thus, it appears that not all surface perturbations become unstable, and the overall appearance of the isolated alcoves is different than the irregular scallops, which develop over a surface melting or dissolving from below.[4,8]

Further comparing the cross sections at different time intervals, we observe that the ceiling recedes the fastest compared to all the other surfaces. We measure the change in the ceiling height as a function of time t for five different examples of spontaneously formed alcoves in our experiments [see Fig. 3(b)]. While there is some variation, the time dependence is more or less similar with essentially linear growth before a slowing down once the alcove reaches the back-wall of the mold at 16.3 ± 0.3 min in the various cases. We, thus, postulate that alcoves start to develop at inverted regions corresponding to

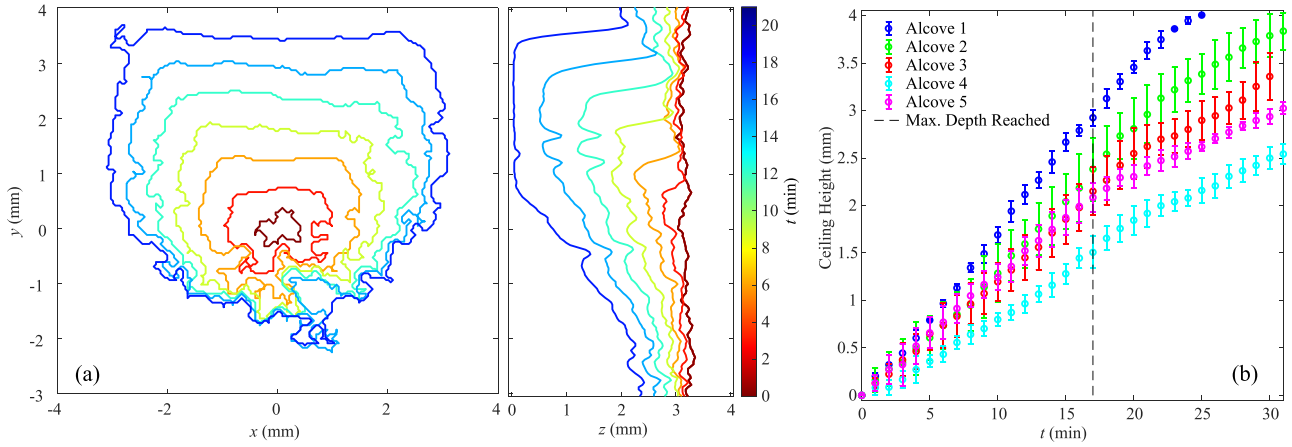

FIG. 3. (a) The alcove outline and vertical mid-profile shows the evolution of the ceiling and floor. The outline correspond to a contour $h = 0.1H$ from the vertical surface, and its roughness is predominantly due to imaging artifacts. (b) The average change in the ceiling height as a function time based on five spontaneously formed alcoves under similar conditions. The ceiling height is located by finding the location of the ceiling edge corresponding to $x = 0$ cm. The ceiling is measured to recede up at a constant rate range between $\dot{\eta} = 6.0$ and $\dot{\eta} = 10.7$ mm/h till the back wall is reached (vertical dashed line) before slowing down. The measured rate averaged over five examples $\dot{\eta} = 8.4$ mm/h is consistent with the estimated rate 9.4 mm/h from Eq. (2) corresponding to a solutal Rayleigh–Bénard instability.

indentations or bubble defects with a critical size, when the ceilings recede rapidly and spread horizontally as the solid dissolves.

IV. BOUNDARY LAYER ANALYSIS

When a solid is immersed in a solvent bath, a concentration gradient of the solute develops at the interface, forming a boundary layer, which grows by diffusion.[21] This boundary layer is stable in gravity when the dissolving interface is below the solution, and the solution density increases with solute concentration. If the dissolving surface is tilted or of finite size, boundary layer flows can develop along the slope under the action of the gravity but remain attached to the solid interface. Such conditions shape the dissolving body at large scales.[14,15,22] In contrast, if the solid is above the solvent bath, a density inversion occurs rapidly as the boundary layer becomes more dense than the solvent below. Thus, gravity can destabilize the boundary layer generating descending plumes similar to the miscible Rayleigh–Taylor instability.[23] Because diffusion and the fluid viscosity can oppose the destabilizing effect of gravity, the concentrated boundary layer becomes unstable only when its thickness exceeds a critical value. Then, the instability is more accurately identified with the solutal Rayleigh–Bénard instability.[8,24] The boundary layer is continuously regenerated by dissolution between the emission of successive plumes, so that its thickness remains on average close to the critical value, as shown experimentally[8,14,16] and numerically.[24] As we argue and demonstrate in the following, this analysis developed on the dissolution of inverted surfaces can be applied here to the ceiling of the alcoves.

While it is not possible for us to directly show the boundary layer, we can visualize the descending plumes when they can be contrasted with a bright background. This is possible by using an alcove with a clear back-wall corresponding to that of the mold. As shown in Fig. 4(a), faint plumes descending from the ceiling can be directly observed in the closeup image and in the associated movie in the supplementary material. Plotting the average intensity across the region marked by the dashed box in Fig. 4(a), we observe 7–8 plumes clearly visible corresponding to an approximate spacing of 2 mm. Similar plumes have been observed descending from spherical candy blocks as well giving rise to nonuniform dissolution of the solid with a smooth top-half surface and a flatter bottom with sharp edges due to flow separation.[14] These plumes rapidly take away the dense solution from the boundary allowing fresh fluid to enter the region and allowing further dissolution to occur. Thus, this instability allows a relatively rapid recession of inverted dissolving boundaries to occur relative to other orientations as noted in Fig. 3(a).

The critical thickness of the concentration boundary layer δ_c that can cause the solutal Rayleigh–Bénard instability between a rigid boundary and a stress-free boundary is given by[8,14]

$$\delta_c = \left(\frac{\mathrm{Ra}_c\, \nu\, \rho_f\, D}{g \Delta \rho}\right)^{1/3}, \tag{1}$$

where $\mathrm{Ra}_c = 1101$ is the critical Rayleigh number corresponding to rigid-free mixed boundary conditions,[23] $g = 9.8\ \mathrm{m/s^2}$ is the gravitational acceleration, $\Delta\rho$ is the density difference across the layer, ν is the kinematic viscosity, ρ_f is the density of the far-field fluid, and D is the molecular diffusion constant of the dissolved species. During the entire dissolution process, the thickness of the concentration boundary layer remains close to its critical value δ_c due to the emission of the plumes. Because the solid–fluid material system is similar to those used in Ref. 14, we follow estimates there that $\Delta\rho = 300\ \mathrm{kg/m^3}$ and $D = 4.3 \times 10^{-10}\ \mathrm{m^2/s}$. Then, assuming a viscosity of the sugar solution averaged between the saturation value ($\nu = 7.7 \times 10^{-4}\ \mathrm{m^2/s}$) next to the solid and water ($\nu = 1.0 \times 10^{-6}\ \mathrm{m^2/s}$) outside the boundary layer, we find $\delta_c \approx 0.40$ mm. The Schmidt number is used to estimate the relative magnitude of momentum diffusivity to mass diffusivity and is given by $\mathrm{Sc} = \nu/D$. Substituting in the viscosity corresponding to water to obtain a lower bound, we have $\mathrm{Sc} \approx 10^3$. Hence, viscosity dominates diffusion, and the solute can be expected to be confined within the boundary layer. Under these conditions, the critical wavelength of the instability $\lambda_c \approx 5\,\delta_c = 2$ mm. This estimate is remarkably consistent with the mean plume spacing seen in the example shown in Fig. 4. Thus, δ_c can provide a critical length scale for an inverted region needed to trigger a flow instability, which can lead to enhanced dissolution. Conversely, smaller perturbations may not be sufficient for the instability to develop and would, thus, smooth out over time as the surface dissolves stably.

The recession rate in terms of the location of the interface η relative to the initial surface is obtained by writing two conservation laws at the interface. The conservation of the mass

$$-\rho_s \frac{d\eta}{dt} = \rho_l \left(\mathbf{u_i} \cdot \mathbf{n} - \frac{d\eta}{dt}\right),$$

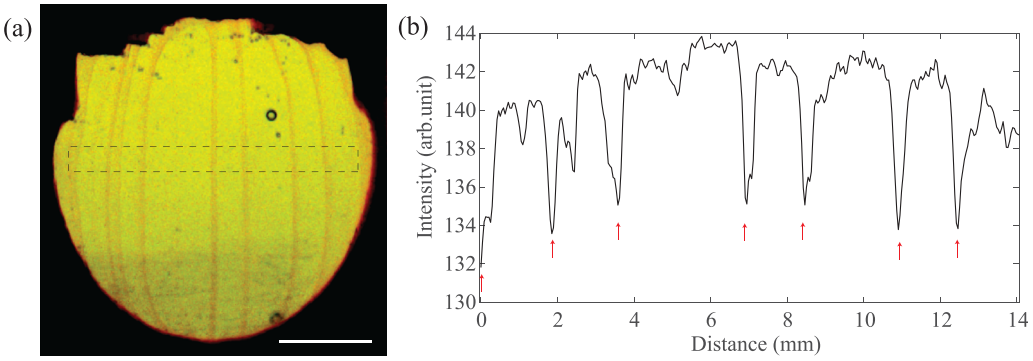

FIG. 4. (a) Image of plumes descending from the ceiling of an alcove ($t = 21$ min). A few stray air bubbles, which appear as small circles, are also visible. The scale bar corresponds to 5 mm. (b) Intensity profiles as a function of the horizontal distance corresponding to the dashed box shown in (a) with locations of plumes indicated by arrows. Average plume spacing is observed to be approximately 2 mm consistent with critical wavelength λ_c estimate corresponding to the solutal Rayleigh–Bénard instability.

with $\mathbf{u_i}$ being the fluid velocity at the interface, $\mathbf{n}$ being a unitary vector normal to the interface, and ρ_l being the density of the liquid at the interface. Then, the conservation of the solute gives

$$\rho_s \frac{d\eta}{dt} = \left(\frac{d\eta}{dt} - \mathbf{u_i}\cdot\mathbf{n}\right) c_i + D\nabla c\cdot\mathbf{n},$$

where c is the mass concentration of the solute in the solution and c_i is the concentration of the solute at the interface. The last term corresponds to the diffusive flux at the interface according to Fick's law. For fast dissolving species, the interface concentration c_i is, to a good approximation, very close to the saturation concentration c_{sat},[24] and thus, the liquid density ρ_l is also close to the saturation density ρ_{sat}. The diffusive flux $D\nabla c\cdot\mathbf{n}$ can be then approximated by $D\,c_{sat}/\delta$ if the bath can be approximated as fresh water. By combining these last two equations, we obtain

$$\frac{d\eta}{dt} = \frac{D\,c_{sat}}{\rho_s\,\delta\,(1 - c_{sat}/\rho_{sat})}, \tag{2}$$

where the saturation concentration of sucrose $c_{sat} = 940$, $\rho_s = 1410\ \mathrm{kg/m^3}$, and the liquid density at saturation $\rho_{sat} = 1300\ \mathrm{kg/m^3}$,[14] while starting with distilled water as the solvent.

Plugging in the diffusion and concentrations corresponding to our experiments, we estimate the solutal Rayleigh–Bénard instability implied recession rate $\dot{\eta} = d\eta/dt = 9.4$ mm/h by then using $\delta = \delta_c$. This estimated value of $\dot{\eta}$ is remarkably consistent with the measured rate ≈8.4 mm/h at which the ceiling recedes up upward in the examples shown in Fig. 3(b). Agreement observed with the plumes, and the recession rate, thus, clearly identifies the nature of the instability leading to alcoves as being consistent with solutal Rayleigh–Bénard instability in our experiments.

V. ALCOVE EVOLUTION

Having established predictions for the conditions under which the alcoves initiate, we next examine the evolution of the alcove opening shape. We simplify and standardize the surface perturbation that leads to alcoves by starting with a cylindrical cavity of radius $R_o = 5$ mm in the center of $L = 60$ mm × $W = 40$ mm × $H = 3$ mm mold, while minimizing the bubble defects in the solid. We place the vertical interface a distance $d_{gap} = 1$ mm parallel to a sidewall of the bath container to simplify imaging, and distilled water is then added to start the dissolution. As long as fluid is allowed to pass across and d_{gap} is greater than the boundary layer flow, the relative location of the dissolving interface in relation to a sidewall is found to have no particular effect on the phenomena of interest.

Figure 5(a) shows the contours in the x–y plane corresponding to a depth of $0.1H$ from the vertical surface in 240 s time intervals to quantify the development of the alcove opening. We observe that the ceiling of the cavity flattens over time, while the bottom tapers and becomes elongated as it grows to resemble the ones seen in Figs. 2(c) and 3(a). Measured from the initial center ($x = y = 0$ cm), the alcove opening develops peaks or triangular corners at approximately $\phi = -20°$ and $\phi = 20°$ relative to the x-axis. Thus, the shape grows rather symmetrically about the flow direction considering the imperfections in the solids. Some imperfections in the shape of the initial circular shape and a few air bubbles can be noted in the images as dissolution progresses. However, these imperfections appear to not affect the evolution of the shape downstream and the overall development of the alcove.

Figure 5(b) shows the area of the alcove opening $A(t)$ enclosed by the contours corresponding to a small depth $h = 0.1H$ from the vertical surface. We observe that $A(t)$ grows increasingly rapidly with time. Further comparing the opening area of the horizontal cavity as a function of time in Fig. 5(b), we observe that it does not grow significantly over the same time interval (see Appendix B). While not circular, the alcove grows in all directions. The recession rate $\dot{\eta}$ given in Eq. (2) is only strictly valid at the inverted alcove ceiling. Nonetheless, we assume that $\dot{\eta}$ provides a first order estimate of the magnitude of the gravity driven dissolution rate all along the alcove contour [see

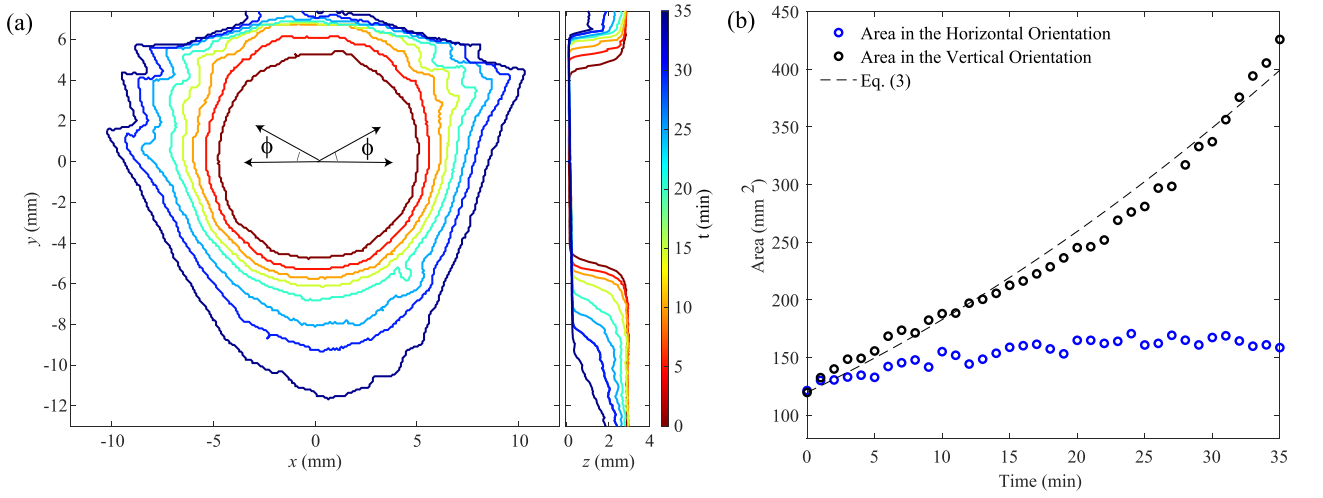

FIG. 5. (a) Contour corresponding to $h = 0.1H$ show the progression of the alcove opening shape and vertical cross section. The angle $\phi = -20° \pm 5°$ and $20° \pm 5°$ at which triangular corners develop are also shown. (b) The area contained with the contour for the case shown vertically, and when a similar initial interface is placed horizontally (see Appendix B). Dissolution progresses much more rapidly when the interface is vertical. A fit to Eq. (3) with $K = 1.647$, 95% confidence bounds (1.609, 1.685), and $R_o = 6.17$ mm is observed to capture the overall increase in alcove opening area in the vertical case surprising well considering that a circular opening is assumed.

Fig. 3(a)]. Then, the opening area of the alcove $A(t)$ as a function of time t can be estimated as

$$A(t) = \pi(R_o + K\dot{\eta}\, t)^2, \tag{3}$$

where R_o is the radius of the indentation at time $t = 0$ and K is a geometric fitting parameter of O(1). This measured area of the alcove enclosed by the contours is plotted along with the fits to Eq. (3) in Fig. 5(b). The fit appears reasonable with $K \approx 1.65$ and $R_o = 6.17$ mm, implying that the average contour expansion speed is essentially constant. (A somewhat larger R_o fit-value is used compared to initially prepared 5 mm circular radius, because the surface starts to dissolve as soon as the mold is placed in the water bath before the imaging starts.) Averaging further over four examples of alcove growth, we find K in the range 1.44 and 2.77. We also compare Eq. (3) with area evolution corresponding to the spontaneously formed alcove shown in Fig. 3(a). As can be seen from Fig. 6, we observe good agreement with $K \approx 1.1$ and $R_o = 0$ cm, since the initial size of a spontaneously formed alcove is negligible. Therefore, $\dot{\eta}$ given in Eq. (2) gives a surprisingly good estimate of the overall alcove opening formed under different conditions, even though the hypothesis of uniform expansion does not apply to the contours at all times. A systematic overestimate may be expected, because the model assumes that the alcove remains cylindrical, whereas the floors are sloped significantly giving rise to a larger area while considering the contour given by $0.1H$. One observes from the central cross sectional view shown in Fig. 5(a) that the transition upstream from the vertical interface above the alcove to the ceiling remains sharp even as it retreats upward. On the other hand, the floor begins to slope and the edge round out, leading to a gradual transition downstream over time.

The evolution of the floor slope may be viewed as being similar to those reported in the development of pinnacles[13,15] as when an attached flow shapes dissolution over large scales. There it was found that the pinnacle tip descends at a rate proportional to the curvature of the tip to the 1/4 power. However, the overall geometries are different because of the convex tip shape in the case of the pinnacles and the concave shape at the base of the alcove. A more recent theoretical study in two-dimensions[22] addresses the shape evolution of a soluble body with an attached boundary layer flow. The predicted shape evolution is qualitatively similar to the floor change plotted in Fig. 5(a) in the y–z plane. Nonetheless, this model does not capture the triangle shape observed experimentally in the x–y plane. Assuming that the thickness of the solid block is the appropriate length scale in our system, we note a faster retreat of the floor downward, as the solid thickness decreases [see Fig. 5(a)]. In contrast, the retreat of the floor downward slows down and even stops over time in the example shown in Fig. 3(a), as the alcove depth increases starting from a small perturbation.

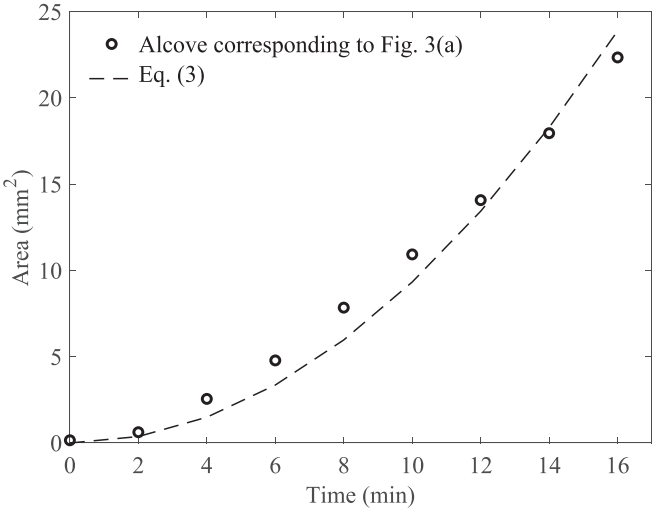

FIG. 6. The alcove opening area corresponding to the example shown in Fig. 3(a). Equation (3) with $K = 1.104$, 95% confidence bounds $(1.073, 1.137)$, and $R_o = 0$ mm is observed to describe the area evolution.

VI. GRAVITY CURRENT AND BOUNDARY SEPARATION

We investigate the impact of the fluid flow on the shaping of the dissolving interface by adding micro-sphere tracers to the solution using a laser sheet with wavelength 532 nm to uniformly illuminate the area of interest. The latex spheres with diameter $d_{ms} = 15\,\mu$ m and density $\rho_{ms} = 1.1$ g/cm^3 fluoresce, and a bandpass filter is placed in front of the camera to block directly reflected light from entering the camera. This enables us to capture an image of the tracers with higher degree of contrast compared to the background. Sucrose was added to the initial bath to match that density while doing these measurements to reduce any settling due to density differences between the tracers and the fluid. While increasing the density of the initial bath may be anticipated to have an effect on progress of the instability from Eq. (1), in practice we find that the measured rate $\dot{\eta} = 7.5$ mm/h is within the range of variations observed in formation of alcoves [see Fig. 3(b)]. Thus, we expect our observations to apply to the examples discussed earlier where the initial bath was sucrose-free.

Figure 7(a) shows an image from the front while de-focusing the laser sheet and illuminating the entire $d_{gap} = 1$ mm fluid gap between the dissolving interface and the front boundary from the side. Figure 7(b) then shows streaks made by the tracers obtained by adding successive images over 2 s long using the maximum intensity function in ImageJ. The flow can be observed not only to be more or less uniformly downward outside the alcove but also converges weakly and then diverges as it passes the alcove. Furthermore, flows in and out of the projected plane are also clearly visible inside the alcove. Thus, it can be noted that while the flow is symmetric about the vertical axis, the flow inside the alcove is asymmetric in the flow direction and does not follow the interface near the ceiling.

To obtain a full picture of the flow, we visualize a central vertical thin ($\approx$100 μm) section through the alcove by swapping the position of the camera and the laser sheet to be from the side and the front, respectively. A movie of the flow can be found in the supplementary material. Figure 7(c) then shows the flow visualized using the tracers over a 2 s time interval in the orthogonal plane. A further zoomed in side view of the region near the ceiling is shown in Fig. 7(d), where the tracers tracked over time are also shown. It is evident that there is clear flow separation as the gravity driven flow detaches from the surface at the edge where the vertical surface meets the ceiling of the alcove before reattaching to the back wall some distance down [see Fig. 7(e)].

From these complementary views, we conclude that the flow has a rich three dimensional structure with a predominantly downward flow, which detaches at the alcove ceiling and reattaches inside the

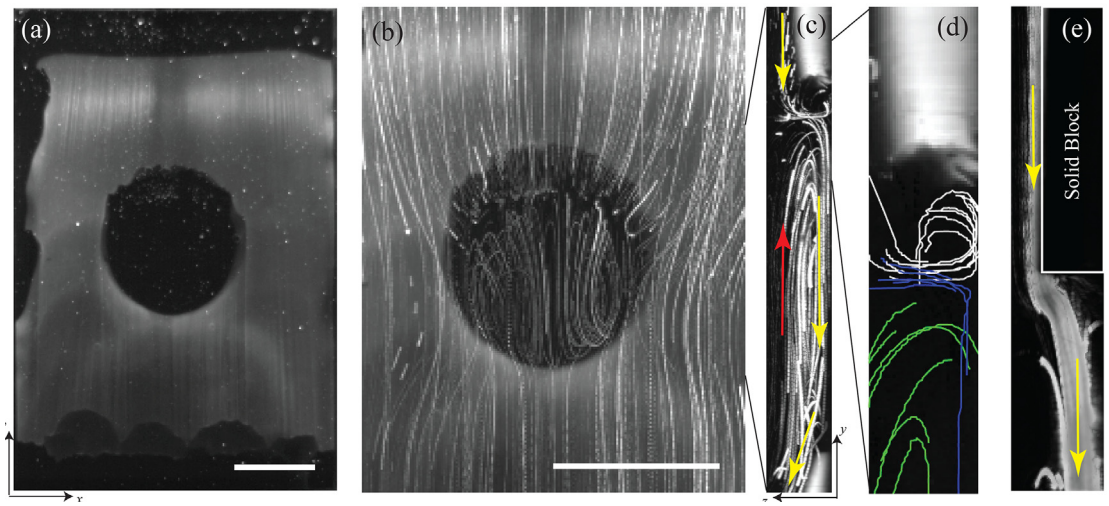

FIG. 7. (a) An image of the partially dissolved surface contained within a 6 $\times$ 4 cm^2 vertically oriented mold at time $t = 20$ min with fluorescent tracers added to visualize flow. (b) A zoomed in view of the fluid flow illustrated by using tracks of the tracers over a $\Delta t = 2$ s time period. A gravity driven downward current is observed along the dissolving surface. Circulation can be also observed inside the alcove. (c) A central alcove cross section showing the circulating currents within the alcove. The flow is observed to detach from the edge where the vertical dissolving surface meets the alcove ceiling. (d) A magnified view of the region containing the counterclockwise rotating vortex observed near the ceiling, the flow reattachment, and the clockwise rotating vortex further downstream with tracer tracks denoted with white, blue, and green colors, respectively. (e) A $\Delta t = 2$ s long exposure image processed with maximum intensity and background subtraction reveals the dominant flow path for the gravity current. The area noted as solid block corresponds to a section of the undissolved sugar block. The white bar in (a) and (b) corresponds to 1 cm, and the width of the sugar block in (c) and (d) corresponds to 3 mm for scale.

back of the alcove before flowing down and out. Furthermore, two sets of circulating currents or vortices are present inside the alcove. One gives rise to a return flow upward in front of the alcove face away from the interface itself. The other, which is located between the ceiling and where the flow detaches from the ceiling, gives rise to flow that is directed outward along the alcove ceiling.

The velocity v_y along the interface was obtained by measuring the average length of the ten longest streaks by eye from movies recorded at 24 frames per second in one minute time intervals over the course of the entire interface dissolution and further averaging over three trails. These speeds in the flowing layer were observed to be right adjacent to the dissolving interface and are no more than a fraction of millimeter in width. The measured speeds are plotted in Fig. 8(a), and observed to be, initially, approximately 2.5 mm/s and then decrease over time. We attribute this decrease in speed to a finite size effect. As the interface dissolves, its total length inside the mold decreases after a few minutes because of relatively faster dissolution of the solid at the top and bottom edge of the mold interface [see Fig. 7(a)]. We quantify this by plotting the total length of the dissolving solid interface through the center in Fig. 8(b) and the fractional length dissolving the solid interface above the alcove in Fig. 8(c). Both can be observed to decrease similarly, and one-to-one correspondence can be noted with the decrease in the flow speed.

To understand this, we can note that the speed of the currents is determined by gravity acting on the solute concentrated solution and the viscous drag of the flow across the interface and through the bath. Because the dissolving part of the interface decreases while the effective length of the recirculating flows through the bath remains unchanged, this can give rise to an overall slowing down of the flow as observed here. The slowing down of the flow due to finite size effects leads to a decrease in alcove ceiling recession as can be noted in the overlap of the contour lines at later times in Fig. 5(a). Thus, the overall flow across the entire interface and the dissolution at the ceiling due to density-inversion are both important to determine the overall evolution of the dissolving interface.

The Reynolds number of the flow is given by $\mathrm{Re} = \rho Ul/\mu$, where ρ is the density of the solution, μ is the kinematic viscosity, U is the velocity scale, and l is a length scale. Then, assuming $\mu > 8.90 \times 10^{-4}$ Pa s, the viscosity of water at 25 °C, and $l \sim H = 0.4$ cm, we have $\mathrm{Re} < 2.4$. Thus, the boundary layer flows in our experiments is in the low-Re laminar flow regime, as also confirmed by tracer motion near the dissolving surface in the movies. At similar low Re numbers, vortices have been reported in the case of flow past a back step[25] and is a result of the momentum of the fluid as it moves past the sharp discontinuity. To quantify the detachment of the flow, we measure the reattachment length L_r from where the flow moves downward next to the wall to the ceiling as shown in the inset of Fig. 8(e). Figures 8(d) and 8(e) show that the step length and the reattachment length of the flow are observed to decrease over time as the solid dissolves. The ratio of the reattachment length and the step size is observed to be roughly similar and constant over the duration of the dissolution as the Reynolds number of the boundary layer flow $\mathrm{Re_{bl}}$ decreases slowly [see Fig. 8(f)]. In calculating $\mathrm{Re_{bl}}$, we have assumed that the relevant density and viscosity of the fluid are that of water, the length scale corresponding to the boundary layer is given by the fast moving layer in Fig. 7(e), which is of order 100 μm, and the flow speed U is given by v_y plotted in Fig. 8(a).

Combining our observations on the evolution of the alcove shape and gravity currents, one can surmise that the alcove shapes evolve because of the two different flows at the ceiling and on the other sides

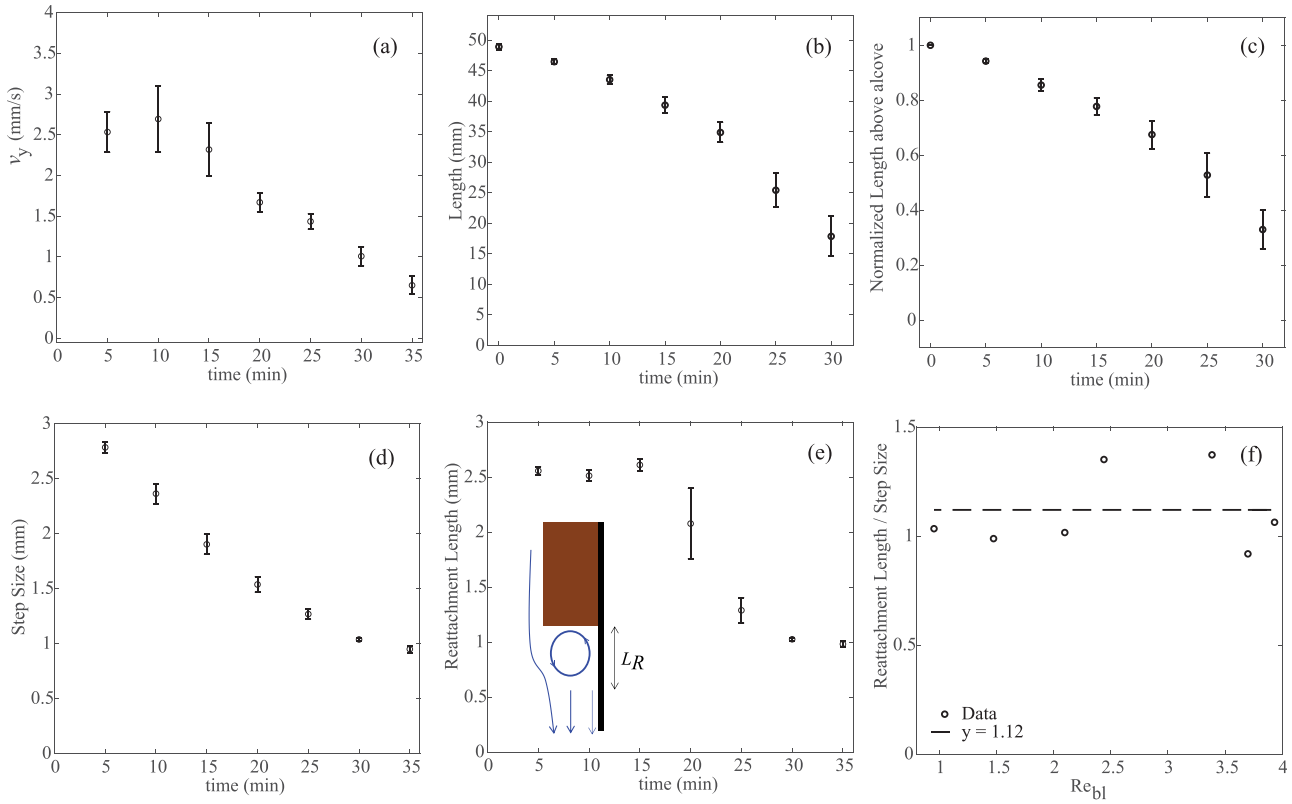

FIG. 8. (a) Average downward velocity of the gravity current along the dissolving vertical surface just above the alcove over time. The data are averaged over five examples, and error bars correspond to the root mean square deviations from the mean. (b) The total length of the interface decreases over time as the solid dissolves leading to the decrease in the gravity current speed. (c) The fraction of the dissolving solid above the alcove also decreases proportionately. (d) The step size corresponding to the thickness of the dissolving solid above the alcove through which the gravity current passes as it enters the alcove region. (e) The reattachment length L_R decreases as the step size decreases over time. Inset: sketch of the flow and the corresponding L_R. (f) The ratio of the reattachment length to the step size remains approximately constant as a function of the boundary layer Reynolds number calculated over the duration of the dissolution. Re_{bl} remains moderate over the entire duration.

of the alcove. The flow separation and the counter-rotating vortex lead to a boundary layer, which preserves the sharp discontinuity as the ceiling dissolves at a rate set largely by the solutal Rayleigh–Bénard instability that causes the ceiling to grow laterally. On the contrary, the flow does not separate from the boundary near the sides, and the floor gives rise to dissolution rates set there by the flow tangential to the surface at those locations. This gives rise to the evolution of the surface, which round out over time giving rise to a gradual change in slopes. Because the dissolution increases with tangential flow, the shapes can be expected to elongate along the flow direction. Hence, this flow can give rise to the smooth conical surfaces below the ceiling that elongate over time.

VII. DISSOLUTION OF SMOOTH AND ROUGH INTERFACES

In complementary experiments, we examined the dissolution of solids with sufficiently smooth surfaces to see if the dissolving interface is indeed stable under otherwise similar preparation and environmental conditions. Solid blocks were prepared to be free of large bubble defects and studied while the dissolving interface is oriented parallel and perpendicular with respect to gravity. No alcoves were observed to grow, and the surfaces remained smooth and planar as they dissolve.

Figure 9(a) shows a plot of the measured dissolved thickness layer $\eta(t)$ corresponding to the two orientations. The recession rate $\dot{\eta}$ is obtained using the slope of the dashed line fitted to the initial increase in $\eta(t)$ and is approximately 5.3 and 0.53 mm/h in the vertical and horizontal cases, respectively. Thus, the dissolution is clearly greater in the case of the vertical orientation, because convective currents that take away the dense solution in the boundary layer are greater compared to the horizontal case. While the dissolution driven current clearly occurs when the interface is vertical, driving the rapid descent of the denser solution, a slower circulation current is set up as well in the horizontal case. The dissolution driven current, thus, occurs because of the finite size of the dissolving surface compared to the bath. Thus, as the sucrose diffuses up, the denser fluid slowly moves to the sides of the bath container as the interface is of finite size relative to the bath container. Thus, even for the horizontal interface, dissolution is not diffusion limited but assisted by convection, albeit much less so compared with a vertical interface.

We then tested the fact that indentations of a critical size are needed to observe the growth of alcoves, and not just heterogeneity, by adding glass beads with a mean diameter of 0.2 mm to the solid. This was accomplished by preparing the hot sucrose liquid with the same recipe as noted earlier, and by adding beads corresponding to a

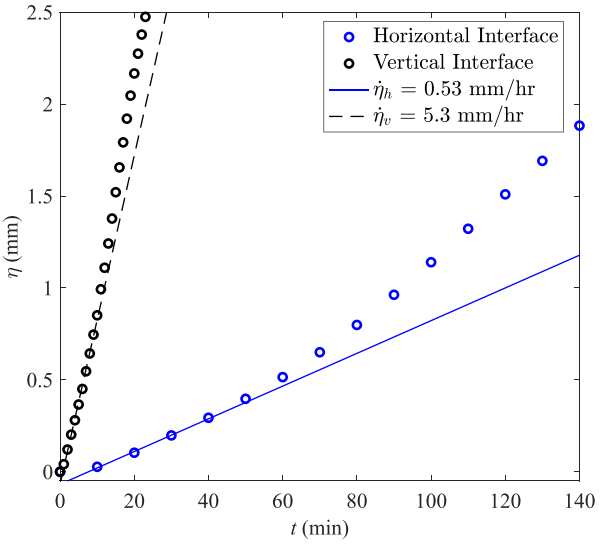

FIG. 9. The average thickness of the solid η measured over time t for the two orientations ($Q_{imp} = 0$ ml/h). The recession rates $\dot{\eta}$ are approximately 0.53 and 5.3 mm/h.

volume fraction $V_f = 0.16$ as it sets. We find that although the glass beads protrude and peel off as the solid dissolves while the interface is oriented vertically, no alcoves form except where trapped air bubbles are present which were of diameter $d_b \gtrsim 0.63$ mm. Alcoves were then observed to develop with inverted triangular shapes and to form at rates similar to those observed without the beads added (supplementary material). It can be noted that this minimal defect size for alcove development is close to the critical size $\delta_c \approx 0.40$ mm needed to trigger the solutal Rayleigh–Bénard instability according to Eq. (1). Thus, indentations caused by trapped bubbles are apparently sufficiently great that the solutal Rayleigh–Bénard instability can develop. The roughness and protrusions due the additional granular phase in these experiments appear to be unimportant to the development of the overall alcove shapes. These data show the robustness of the alcove feature even in the presence of additional non-dissolving solids as is often the case in natural sediments.

VIII. DISCUSSION AND CONCLUSIONS

We have demonstrated that alcoves can develop on vertical solid–fluid interfaces as the solid phase dissolves when indentations of a critical size are present on the surface. Unlike previous demonstrations of scallop-like indentations that cover the undersides of dissolving surfaces, these features are isolated, and small perturbations and protrusions are polished away as the interface dissolves. The alcoves are shown to develop starting at inverted surfaces (or ceilings) of sufficient size as they dissolve leading to a boundary layer with a higher density compared to the solution below. From the observation of plumes descending from the ceiling, their spacing, and the observed recession rate of the ceiling, we deduce that the instability occurs when the boundary layer exceeds a length scale set by the critical Rayleigh number corresponding to mixed boundary conditions. Thus, we identify the mechanism that leads to the formation of alcoves as being driven by the solutal Rayleigh–Bénard instability as a result of the balance between the diffusion of the solute and the buildup of the boundary layer density due to dissolution.

By visualizing the fluid phase near the dissolving interface, we demonstrate that a gravity current develops as the density of solution increases with solute concentration along the entire dissolving interface and not just at the ceiling. As the fluid sinks, fresh fluid from the bath replaces it, and thus, a rapid gravity current is setup moving downward along the interface. We show that the boundary layer flow is in the low-Reynolds number laminar regime, and a boundary flow separation occurs at the edge where the vertical interface meets the ceiling of the indentations, which enforces the discontinuous change in slope at the leading edge of the indentation. The resulting dissolution as a result of the solutal Rayleigh–Bénard instability and the direction of the vortex which develops past the ceiling inside the indentation appear to work in concert to maintain the sharp edge and widening of the ceiling as it continues to retreat upward along the vertical interface. The continuing fluid flow down the side and floor of the indentation remain attached to the surface and serve to smooth sharp edges downstream leading to a gradual change in slope. The combination of density inversion instability at the ceiling and the shaping of the dissolving surfaces by the boundary layer flow result in the triangular shaped alcove with a wide ceiling and a sloping back and floor. The evolution of these shapes is found to be robust even when additional heterogeneity in the form of non-dissolving glass beads is present in the solid phase. The sharp features that start to appear in the ceiling of the alcove, as seen in Fig. 4(a), may be precursors to scallops patterns due to convection flows reported on flat dissolving surfaces[14] and analogous to scallops observed in melting ice over larger length and time scales.[12,26]

While our conclusions are based on fast dissolving sugar-based solids, which are more similar in solubility to rock salts, we anticipate that our results may be relevant as well to slower dissolving rocks such as gypsum and limestone. The relative effect of chemical dissolution rate and diffusion on solutal convection have been recently investigated numerically by Philippi *et al.*[24] They find that a concentrated layer near the interface still develops and convection sets in with emission of plumes for sufficiently large density inversion even though saturation is not reached. Practically, this means that the characteristic length scale given in Eq. (1) will be larger, and the time scales set in Eq. (2) longer in slower dissolving rocks.

Although the flow geometry is quite different than in confined triangular cavities that occur inside salt deposits studied by Gechter *et al.*,[9] an analogy can be observed. The appearance of dissolution at the ceiling due to the solutal Rayleigh–Bénard instability leads to an efficient transfer of the dissolved solute to regions where flow is rapid in turn giving rise to the triangular shapes. The flows in and out the alcove are, however, different than those in the formation of conical enclosed cavities in salt deposits. The rapid gravity currents over the entire open interface further shape the dissolving boundary leading to a recession of the alcove floor with a slope downward polished by the attached boundary layer flow consistent with recent studies of dissolving pinnacles.[14,22] Further modeling is needed to draw quantitative comparisons between features observed in these various interfaces shaped by dissolution and flow.

Finally, we note that our two-phase physical model system is highly simplified compared with alcoves observed in nature. Natural cliffs have far more complex rock chemistry and heterogeneity and can experience a wide range of physical weathering from temperature

variation to rain and wind besides chemical and biological weathering. Dissolution by surface runoffs fed by rainfall may play a role in the initiation of surface patterns.[27] Nonetheless, recent experiments with dissolving solids in an aqueous bath demonstrate that convective dissolution reproduces the shape of the pinnacles created by the rain in Karst regions.[13] In these studies, as in ours, dissolving sugar results in considerable variation in viscosity and diffusivity, which is not the case in typical rock dissolution. The universality of the overall alcove shapes that evolve, largely independent of initial conditions in our system points to the underlying robustness of such features in dissolving solids shaped by gravity driven boundary layer flows. Exploring these connections more deeply remains an avenue for further research.

SUPPLEMENTARY MATERIAL

See the supplementary material for movies of the dissolution dynamics. Movies show the formation of alcoves, and the flows can be found in supplementary material videos: S1: The time-lapse movie of alcove formation starting from sugar block immersed in an aqueous bath with a vertical dissolving interface. The images are taken 1 min apart, and the time duration corresponds to 26 min. S2: the movie illustrating plumes descending from the alcove ceiling against a bright background. The movie corresponds to 20 min and starts 5 min after a solid block with a 1 cm cavity is immersed in an aqueous bath. S3: Cross sectional view of an alcove and flow illustrated by adding fluorescent spheres to the bath. The movie corresponds to images acquired at 24 frames per second over a 5 s time interval 5 min after a vertical interface with a 1 cm diameter cavity is immersed in the bath. S4: Dissolution of a solid vertical interface with non-dissolving 200-μm solid glass beads added to increase heterogeneity. Alcoves are initiated where air bubbles of sufficient size are also present. The movie corresponds to 40 min and images are taken every 1 min. The scale bar corresponds to 5 mm. S5: A horizontal interface with a 1-cm circular cavity dissolves uniformly in contrast with a vertical interface. A fluid flow with a mean speed of 0.7 mm/s is imposed across the interface using a syringe pump from left to right. The movie corresponds to 137 min with images taken every 10 min. Scale bar corresponds to 5 mm.

ACKNOWLEDGMENTS

This research was supported by the U.S. Dept. of Energy, Office of Science, Basic Energy Sciences under Grant No. DE-SC0010274.

AUTHOR DECLARATIONS

Conflict of Interest

The authors have no conflicts to disclose.

DATA AVAILABILITY

The data that support the findings of this study are available within the article and its supplementary material.

APPENDIX A: IMAGING

To map the observed intensity to the height of the dissolving solid, we prepared a system with two cameras configured as shown in Fig. 10(a) to simultaneously acquire images. The solid in mold is placed horizontally in a bath of distilled water. As the solid dissolves, the concentrated mixture settles on top of the undissolved solid. This mixture is displaced using a Pasteur pipette filled with distilled water to keep the bath water near the interface from changing color due to the high concentration of the dissolved solute. Images of the cleaned surface are then acquired every 5 min. Camera 1 placed directly above the dissolving solid captures the intensity corresponding to the solid sugar. Camera 2 placed at a grazing angle captures the wall of the mold as it becomes visible. Since we know the dimensions of the mold when filled with the dissolving solid and without any dissolving solid present, we use this configuration to determine the actual height of the mold wall becoming visible. Consequently, we determine the height of the dissolving solid. Since these are imaged simultaneously, we can compare the height of the solid at a given time with the average intensity observed at that same time. These data are plotted in Fig. 10(b) and are described by the function $I(h) = 14 + 180\exp(-0.8\,h)$, where the thickness of the block is greater than 0.1 mm, consistent with the Beer–Lambert law with a uniform light attenuation through the solid.

APPENDIX B: HORIZONTAL INTERFACE

To understand the conditions under which these features grow, we also examine the dissolution dynamics with a similarly prepared interface, while placed horizontally as shown schematically in Fig. 11(a). A flow of $Q = 100$ ml/h, corresponding to an average speed of 0.7 mm/s initially, similar in order of magnitude as

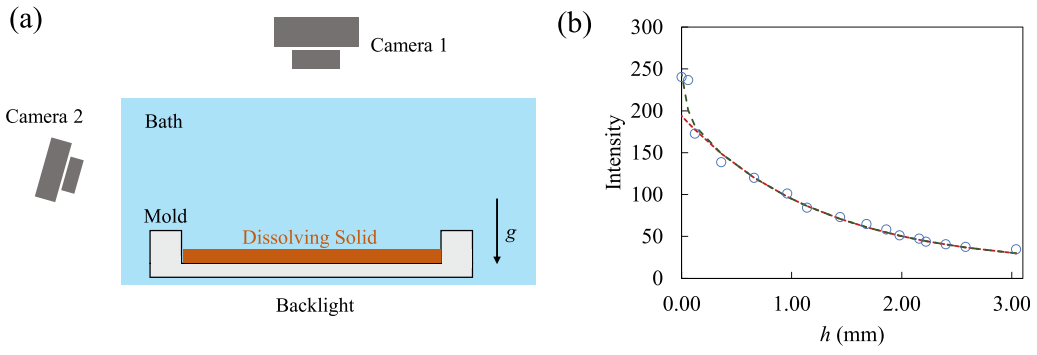

FIG. 10. (a) Schematic of the system used for calibrating the light intensity to solid thickness h. (b) Light intensity measured as a function of solid thickness h. An exponential fit is found to describe the data for $h > 0.1$ mm.

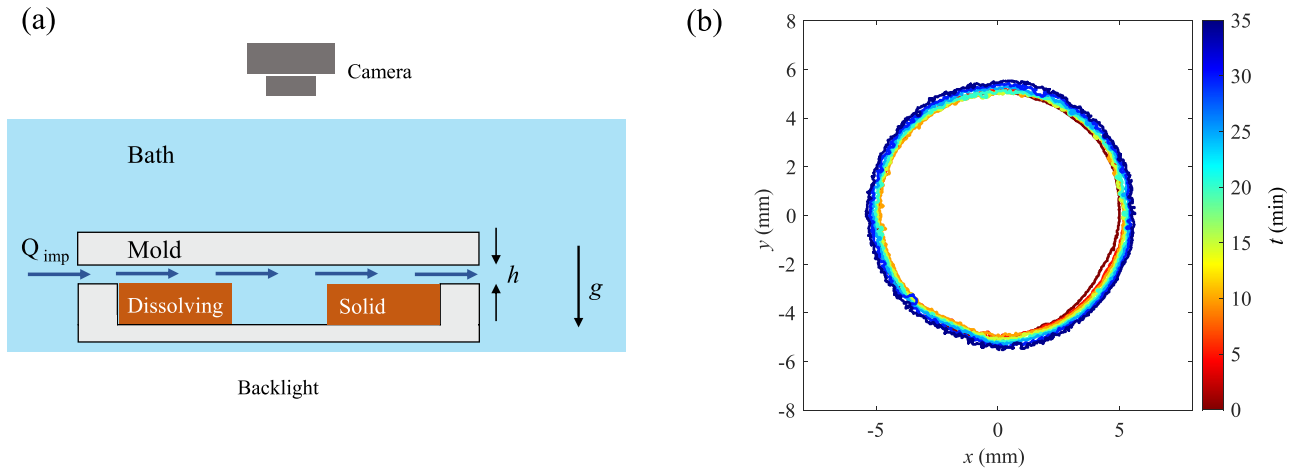

FIG. 11. (a) Schematic of the experimental system used to measure the dissolution of the interface when placed horizontally in the bath. A syringe pump is used to impose a flow across the interface with a prescribed rate. (b) Contour plot of the cavity development as a function of time corresponding to $Q_{imp} = 100$ ml/h. The cavity remains circular.

those which arise near a vertical interface, is imposed across the horizontal interface to create a flow across the interface and flush out the dissolved sugar. The dissolution occurs relatively faster, in 2 h (135 min), compared to when no flow is imposed. Nonetheless, the cavity evolves uniformly. As can be seen from the contour line plots in Fig. 11(b) and the movie in the supplementary material corresponding to the entire 2-h duration, the interface dissolves more or less uniformly, and the cavity does not grow significantly in diameter even as the entire solid dissolves. Thus, it is not just the presence of surface perturbation, which is important to the formation of the triangular shaped alcoves but also the orientation of the interface.

REFERENCES

[1]C. N. Fredd and H. Scott Fogler, "The kinetics of calcite dissolution in acetic acid solutions," Chem. Eng. Sci. **53**(22), 3863–3874 (1998).
[2]P. J. Ortoleva, *Geochemical Self-Organization* (Oxford University Press, New York/Clarendon Press, Oxford, 1994).
[3]M. C. Malin and K. S. Edgett, "Evidence for recent groundwater seepage and surface runoff on mars," Science **288**(5475), 2330–2335 (2000).
[4]P. Meakin and B. Jamtveit, "Geological pattern formation by growth and dissolution in aqueous systems," Proc. R. Soc. A **466**, 659–694 (2010).
[5]A. Kudrolli and X. Clotet, "Evolution of porosity and channelization of an erosive medium driven by fluid flow," Phys. Rev. Lett. **117**, 028001 (2016).
[6]D. J. Jerolmack and K. E. Daniels, "Viewing Earth's surface as a soft-matter landscape," Nat. Rev. Phys. **1**, 716–730 (2019).
[7]D. G. Thomas and R. A. Armistead, "Concentration-gradient-driven convection: Experiments," Science **160**(3831), 995 (1968).
[8]T. S. Sullivan, Y. Liu, and R. E. Ecke, "Turbulent solutal convection and surface patterning in solid dissolution," Phys. Rev. E **54**, 486–495 (1996).
[9]D. Gechter, P. Huggenberger, P. Ackerer, and H. N. Waber, "Genesis and shape of natural solution cavities within salt deposits," Water Resour. Res. **44**(11), W11409, https://doi.org/10.1029/2007WR006753 (2008).
[10]J. M. Huang, M. N. J. Moore, and L. Ristroph, "Shape dynamics and scaling laws for a body dissolving in a fluid flow," J. Fluid Mech. **765**, R3 (2015).
[11]E. Nakouzi, R. E. Goldstein, and O. Steinbock, "Do dissolving objects converge to a universal shape?," Langumir **31**, 4145–4150 (2015).
[12]C. Cohen, M. Berhanu, J. Derr, and S. Courrech du Pont, "Erosion patterns on dissolving and melting bodies (2015 gallery of fluid motion)," Phys. Rev. Fluids **1**, 050508 (2016).
[13]J. M. Huang, J. Tong, M. Shelley, and L. Ristroph, "Ultra-sharp pinnacles sculpted by natural convective dissolution," Proc. Natl. Acad. U. S. A. **117**, 23339–23344 (2020).
[14]M. S. Davies Wykes, J. M. Huang, G. A. Hajjar, and L. Ristroph, "Self-sculpting of a dissolvable body due to gravitational convection," Phys. Rev. Fluids **3**, 043801 (2018).
[15]S. S. Pegler and M. S. Davies Wykes, "Shaping of melting and dissolving solids under natural convection," J. Fluid Mech. **900**, A35 (2020).
[16]C. Cohen, M. Berhanu, J. Derr, and S. Courrech du Pont, "Buoyancy-driven dissolution of inclined blocks: Erosion rate and pattern formation," Phys. Rev. Fluids **5**, 053802 (2020).
[17]M. Bushuk, D. M. Holland, T. P. Stanton, A. Stern, and C. Gray, "Ice scallops: A laboratory investigation of the ice-water interface," J. Fluid Mech. **873**, 942–976 (2019).
[18]S. Weady, J. Tong, A. Zidovska, and L. Ristroph, "Anomalous convective flows carve pinnacles and scallops in melting ice," Phys. Rev. Lett. **128**, 044502 (2022).
[19]J. M. Huang and N. J. Moore, "Morphological attractors in natural convective dissolution," Phys. Rev. Lett. **128**, 024501 (2022).
[20]G. S. Frankel, "Pitting corrosion of metals: A review of the critical factors," J. Electrochem. Soc. **145**(6), 2186–2198 (1998).
[21]F. H. Garner and J. M. Hoffman, "Mass transfer from single solid spheres by free convection," AIChE J. **7**(1), 148 (1961).
[22]S. S. Pegler and M. S. Davies Wykes, "The convective Stefan problem: Shaping under natural convection," J. Fluid Mech. **915**, A86 (2021).
[23]S. Chandrasekhar, *Hydrodynamic and Hydromagnetic Stability* (Clarendon Press, Oxford, 1961).
[24]J. Philippi, M. Berhanu, J. Derr, and S. Courrech du Pont, "Solutal convection induced by dissolution," Phys. Rev. Fluids **4**, 103801 (2019).
[25]T. Matsui, M. Hiramatsu, and M. Hanaki, "Separation of low Reynolds number flows around a corner," in Symposia on Turbulence in Liquids, 1975, Vol. 30.
[26]L. Solari and G. Parker, "Morphodynamic modeling of the basal boundary of ice cover on brackish lakes," J. Geophys. Res. **118**(3), 1432–1442, https://doi.org/10.1002/jgrf.20115 (2013).
[27]A. Guerin, J. Derr, S. Courrech du Pont, and M. Berhanu, "Streamwise dissolution patterns created by a flowing water film," Phys. Rev. Lett. **125**, 194502 (2020).